Z. Phys. Chem. **220** (2006) 349–369 / **DOI** 10.1524/zpch.2006.220.3.349

Hydrophobic Interactions by Monte Carlo Simulations

By Orkid Coskuner* and Ulrich K. Deiters**

Institute of Physical Chemistry, University of Cologne, Luxemburger Str. 116, D-50939 Köln, Germany

(Received December 13, 2005; accepted January 11, 2006)

Hydrophobic Interactions / TIP5P / Chemical Potential / Water / Computer Simulation

The structural and thermodynamic properties of liquid water and of the dilute solutions of methane and ethane in water were calculated by Monte Carlo simulations in the temperature range 298 K to 318 K and 298 K to 333 K, respectively. The nonpolar molecules were modeled as one- and two-center Lennard–Jones particles; for the interaction potential of water a modified TIP5P model was used. The results indicate that the nonpolar solutes tend to aggregate with increasing temperature. Methane molecules preferably form water-separated pairs, even at higher temperatures, whereas for ethane contact pairs are more likely. For the thermodynamic conditions studied here, the residual chemical potential of water is a linear function of temperature.

1. Introduction

The term "hydrophobic interaction" refers to the structural and energetic response of water in the vicinity of hydrophobic solutes. It describes the interaction of nonpolar molecules with water, each other and the interaction between water molecules in the presence of two or more nonpolar molecules.

Because of the low solubility of nonpolar compounds in water, experimental studies of hydrophobic interactions are rather difficult [1–3]. This low solubility results from the fact that the transfer of nonpolar molecules from the gas phase into an infinitely diluted solution involves an increase of the Gibbs energy. At ambient temperature, this Gibbs energy change is a combination of a small decrease in enthalpy and a larger decrease in entropy,

* Recent address: National Institute of Standards and Technology, Physical and Chemical Properties Division, 100 Bureau Drive, Mail Stop 8380, Gaithersburg, MD 20889, USA. E-mail: orkid.coskuner@mail.nist.gov

** Corresponding author. E-mail: ulrich.deiters@uni-koeln.de

as was observed by Butler *et al.* [4, 5]. Most structural theories proposed to account for the thermodynamic observations are based on the idea that a nonpolar molecule increases the degree of hydrogen bonding of water molecules in its solvation shell [6], and that this gives rise to an increased water–water attraction. This explanation of the thermodynamic observations by the formation of ordered structures around nonpolar molecules was nicknamed "iceberg hypothesis" and became a central feature for the description of hydrophobic interactions [7]. Several authors observed a proportionality between the number of water molecules in the surface layer and the free energy, enthalpy, or entropy of solvation [8, 9]. The number of water molecules in the first hydration shell is also a key parameter for the theoretical treatment of aqueous solutions, *e.g.*, in the significant structure theory of Eyring and coworkers [10] or the Némethy–Scheraga model [9]. Current literature also contains discussions of the temperature dependence of the structural properties [11–13].

Theoretical and computer simulation studies provided a valuable insight into the nature of hydrophobic interactions, especially for the association of hydrophobic species. Here it turned out that association can occur in two different ways. Either it can produce contact pairs (nonpolar molecules in immediate contact) or solvent-separated pairs. The approximate integral equation by Pratt and Chandler was the first theory that demonstrated the existence and importance of solvent-separated nonpolar pairs [14]. When attractive forces are added to this theory, two additional effects are noted: First, the enthalpy of association is in closer agreement with the traditional view and second, contact pairs are destabilized [14, 15].

Pangali *et al.* calculated the potential of mean force of Lennard–Jones solutes in water and found agreement with the Pratt–Chandler theory [16, 17]. Other attempts to determine the free energy of association of nonpolar molecules predicted stable solvent solvent-separated configurations [12, 18, 19]. Smith and Haymet calculated the potential of mean force for methane molecules in water and concluded that contact-pairs are more stable than solvent-separated pairs [20]. From molecular dynamics simulations Mancera and Buckingham reported an increased tendency for methane molecules to form contact pairs with increasing temperature [21]. The simulations of Dang showed no such effect, and he therefore attributed the temperature dependence reported in other publications to density effects [22]. Lüdemann *et al.* investigated the temperature dependence of the free energy by computer simulation, using the parameters of Pratt and Chandler, and found a global minimum at contact distance for methane-like molecules [23]. Hernández-Cobos *et al.* pointed out that the early simulations seemed to support the theory of water structure enhancement, but that it would not be the case for the water–methane system according to their computer simulations, where the interactions led to a negative free energy [24].

The temperature dependence of hydrophobic interactions was also investigated by Skipper *et al.*, who simulated four methane molecules in water

at a fixed density and concluded that the association tendency of methane molecules increases with temperature between 275 and 317 K [25, 26]. Some scientists pointed out, however, that these results contain some ambiguity because of methane–methane interactions [27].

Computer simulations require intermolecular potentials, and consequently much effort went into the development of intermolecular potential functions for the water dimer. The number of publications dealing with such potential functions is rather large. One of the earliest is that of Bernal and Fowler [28]; among the first to be used in computer simulations were those of Popkie *et al.* [29] and Stillinger and Rahman [30]. Some recent intermolecular potentials are largely based on quantum mechanical calculations, *e.g.*, those of Kim *et al.* [31], Schwegler *et al.* [32], or Coutinho *et al.* [33]. Special importance attained the "transferable interaction potentials" of Jorgensen and coworkers, TIPS, TIP3P, TIP4P, and TIP5P [34–36].

One of the best known properties of liquid water, which therefore serves as a benchmark for the quality of intermolecular potentials for water, is the density as a function of temperature or pressure. Water exhibits a density maximum at about 277 K and normal pressure [37–39]. However, none of the water models available in the current literature can reproduce this feature in the temperature range of interest; the only exception is the TIP5P (5-site Transferable Intermolecular Potential Function) model proposed by Mahoney and Jorgensen [36]. The TIP5P model represents not only the density maximum near 0.1 MPa, but also the pressure dependence of many thermodynamic properties, *e.g.*, the density of water at 298.15 K is reproduced with an average of about 2% up to 1 GPa. Furthermore, the expected shift of the temperature of maximum density to lower temperatures could be obtained with this model. However, these good results could not always be reproduced. Recent computer simulation studies in which Ewald sum method was applied to the long-range interactions reported smaller densities for TIP5P water [40, 41]. Paschek was able to reproduce the accepted density data for TIP4P and SPCE water, but not for TIP5P water. We observe, however, that his chemical potential data, obtained with the Widom insertion method, do not agree with experimental data.

The principal difficulty in calculations of the chemical potential by computer simulations is the lack of a corresponding microscopic analogue, *i.e.*, a function of configuration space variables to be averaged to obtain the required result. Much effort went into the development of computation methods that worked around this difficulty, such as thermodynamic integration, particle insertion, particle deletion, umbrella sampling and perturbation methods (an overview is given by Frenkel and Smit [42]). Currently no single method for chemical potential simulation can be considered as clearly superior to others.

In this work we present Monte Carlo simulation results for the liquid densities, chemical potentials, enthalpies, and structural properties of water. Three different methods for the calculation of chemical potentials were used and

compared. In order to study hydrophobic effects, further simulations were performed in which two methane or ethane molecules were added to the water. Structural and thermodynamic data were obtained from which the amount of hydrophobic association can be seen, either of contact pairs or solvent-separated pairs.

2. Methods

2.1 Interaction potentials

The TIP5P model for water, developed by Mahoney and Jorgensen [36], consists of a Lennard–Jones center representing the oxygen atom as well as two positive and two negative point charges representing the hydrogen atoms and the lone electron pairs. The four point charges form a distorted tetrahedron. The authors adjusted the oxygen–lone pair distance, r_{OL}, and the partial charges in order to obtain a dipole moment of 7.34×10^{-30} C m and a dimerization energy between -25.0 and -27.2 kJ/mol. Extensive Monte Carlo simulations performed by the authors for several alternative models showed that a minimal change of r_{OL} can greatly influence the macroscopic properties of water [36, 43]. While Mahoney and Jorgensen showed that a r_{OL} of 0.7 Å yields density and potential energy diagrams in agreement with the experimental data, other thermodynamic properties with this model differ from experimental values at higher temperatures.

In order to improve the representation of thermodynamic properties, the TIP5P model was modified: Starting from the original TIP5P model, the oxygen–lone pair distance was allowed to vary between 0.65 and 0.7 Å. The negative charges were moved towards the oxygen, and the Lennard–Jones parameters were varied, too. These modified geometries were then used in the *ab initio* calculations (performed with Gaussian98™ [44]), using Møller–Plesset perturbation theory at the MP2 level with the 6-311G(d+p)) basis set, to determine the dimerization energies and the dipole moments. Using the same procedure as Mahoney and Jorgensen, the density, internal energy, and chemical potential of liquid water were then obtained by computer simulation. By an extensive calculation the internal energies of the water models as well as the deviations of the thermodynamic properties from experiment were minimized. The water monomer with a oxygen–lone pair distance, r_{OL}, of about 0.69 Å and bond angles $\theta_{\mathrm{LOL}} = 109.45^\circ$ and $\theta_{\mathrm{HOH}} = 104.5^\circ$ yielded thermodynamic properties which are closer to the experimental values. The geometric properties and fitted parameters of this model as well as those of original TIP5P model are presented in Table 1.

For this model the dimerization energy is -28.2 kJ/mol and the dipole moment 7.65×10^{-30} C m. The original TIP5P model yields a lower dimerization energy of about -28.4 kJ/mol and a dipole moment of 7.38×10^{-30} C m. All modified models with r_{OL} values between 0.65 and 0.7 Å yield dimeriza-

Table 1. Parameters of the modified and original TIP5P interaction potential of water. Subscript "L" refers to the negative point charges representing the lone electron pairs of oxygen.

parameter	original [36]	this work
q_H/e	0.241	0.239
σ_O/Å	3.120	3.117
ϵ_O/kJ mol^{-1}	0.669	0.669
r_{OH}/Å	0.957	0.957
θ_{HOH}	104.520°	104.500°
r_{OL}/Å	0.700	0.693
θ_{LOL}	109.470°	109.540°

Table 2. OPLS parameters of nonpolar compounds [47].

parameter	methane	ethane
σ/Å	3.730	3.775
ϵ/kJ mol^{-1}	1.230	0.866
r_{CC}/Å		1.530

tion energies between -28.07 and -28.4 kJ/mol and dipole moments varying between 7.52×10^{-30} and 7.79×10^{-30} C m. The experimental results are -22.61 kJ/mol and 6.21×10^{-30} C m, respectively [45, 46]. The difference between these values and the TIP5P results are partially due to the fact that the latter are effective pair potentials optimized for the simulation of liquid water. Furthermore, recent *ab initio* calculations by Coutinho *et al.* with the same molecular geometry, but different basis sets yielded a dipole moment of 7.79×10^{-30} C m with 6-31G(d+p), which agrees with our result, and a value indistinguishable from the experimental one with aug-cc-pVDZ [33]. Aside from these differences, the TIP5P model for water yields structural and thermodynamic properties for liquid water, which are in agreement with experimental data.

OPLS parameters were chosen for methane and ethane, *i.e.*, methane is represented as a single Lennard–Jones center, and ethane as 2-center Lennard–Jones particle [47]. The Lennard–Jones parameters for methane and ethane are displayed in Table 2. Lorentz–Berthelot combining rules were used for the interaction between unlike molecules:

$$\begin{aligned} \sigma_{AB} &= \frac{1}{2}(\sigma_{AA} + \sigma_{BB}) \\ \epsilon_{AB} &= (\epsilon_{AA}\epsilon_{BB})^{1/2} \end{aligned} \tag{1}$$

where A and B stand for water and methane or a methyl group, respectively.

2.2 Simulation details

An isobaric–isothermal ensemble Monte Carlo program, HYDRO, was developed to investigate the hydrophobic interactions. The program uses periodic boundary conditions and the minimum image convention. Acceptance or rejection of trial configurations is decided by Metropolis criteria. Coulombic interactions are taken into account by the Ewald sum method [48]. For this work conducting boundary conditions, a (variable) screening parameter of $6/L$, and a Fourier space vector $\boldsymbol{k} = 10\pi/L$ were used, with the box length L depending on density and fluctuating during the simulation. From the Monte Carlo simulations the pair correlation functions, density, potential energy, enthalpy and residual chemical potentials of water and of the nonpolar molecules were obtained. The residual chemical potential of water was calculated by three different methods, namely the Widom insertion method, the Widom deletion method and the particle deletion method by Boulougouris *et al.* [49–52].

The Widom insertion method requires the addition of a particle to the system and averages over the energy difference between a system with N and $N+1$ particles [49]. The Widom deletion method is based on the comparison between the free energies of a system with N and $N-1$ particles [50, 51]. Recently, Boulougouris *et al.* presented a new formulation of the chemical potential based on the removal of a test particle scheme [52]. This particle deletion scheme is based on the observation that, after the deletion of a particle, the $N-1$ molecules can never occupy the remaining hole, which produces a bias in the Widom deletion method. To remove this bias, Boulougouris *et al.* determined the difference between N and $N-1$ particle systems by calculating the accessible volume for inserting a hard sphere into the system. This method is based on the following chemical potential calculation definition:

$$\beta\mu = \beta\mu^{\mathrm{ig}} - \ln\left(\left\langle\frac{1}{V}\right\rangle\frac{Z(N,\,p,\,T)}{Z(N-1,\,p,\,T)}\right) . \tag{2}$$

Here μ^{ig} represents the chemical potential of an ideal gas under same conditions. The intermediate system of $N-1$ molecules and one hard sphere is introduced via a ratio of the configurational integrals:

$$\beta\mu = \beta\mu^{\mathrm{ig}} - \ln\left[\frac{\langle V^{-1}\rangle_{N,p,T}\,\langle\Pi_{i=1}^{N-1}H(r_i,\,N)\rangle_{N-1,p,T}}{\langle\Pi_{i=1}^{N-1}H(r_i,\,N)\exp\left(\beta U_N(r_i\ldots r_N)\right)/V\rangle_{N,p,T}}\right] . \tag{3}$$

Here the ratio of the configurational integrals is written in terms of Heaviside step functions:

$$H(r_i,\,N) = \begin{cases} 0 & \text{for } |\,r_i - r_N\,| < d_{\mathrm{core}}(\beta,\,p) \\ 1 & \text{for } |\,r_i - r_N\,| \geq d_{\mathrm{core}}(\beta,\,p) \end{cases} . \tag{4}$$

The term $\Pi H(r_i,\,N)$ represents the accessible volume fraction for a molecule of diameter d_{core} that is interacting through a repulsive potential [52].

The residual chemical potential of pure water with the modified TIP5P was calculated by the three different methods described above. For the calculations with the original TIP5P model only the Widom insertion method was used. The simulations were performed with 216 particles at temperatures between 298.15 and 318 K at a pressure of 0.1 MPa.

Simulation runs for the study of hydrophobic interactions were made with 216 water molecules and 2 nonpolar molecules. A real cut-off of 10 Å was applied to short-range interactions, with long-range corrections for molecules at larger distances. Preferential sampling was used for water molecules within 5.5 Å of methane and 6.0 Å of ethane to improve coordination number statistics for the hydration shell region [48]. The simulations consisted of 2×10^6 equilibration moves, followed by 9×10^6 production moves for pure water and 12×10^6 production moves for the water–methane and water–ethane systems. The statistical uncertainty was calculated by using block average analysis, where each run was subdivided into 100 blocks.

The coordination numbers were calculated as integrals over the correlation functions [48],

$$N_c = 4\pi\rho \int_0^{r_{min}} r^2 g(r) \mathrm{d}r \,, \tag{5}$$

where ρ is the number density.

As long as the vapor pressure is low, the heat of vaporization of pure liquid water can be obtained from the simulated potential energy with reasonable accuracy through the following approximation:

$$\Delta_{vap} H \approx -U_m + RT \,. \tag{6}$$

3. Results and discussion

3.1 Pure liquid water

Table 3 contains simulation results for the molar volume V_m, the heat of vaporization $\Delta_{vap}H$, the residual enthalpy H_{res} and the chemical potential of pure water for different temperatures, along with experimental data [53].

The modified TIP5P water yields a density of 0.997 g/cm^3 at 298.15 K and 0.1 MPa. This result is indistinguishable from the experimental value. The simulations with the original TIP5P model by Paschek gave a slightly lower value of 0.982 g/cm^3 at 300 K [41]. From that publication an enthalpy of -39.7 kJ/mol can be derived using the basic thermodynamic relationship $H = U + PV$. In contrast to this, the molar enthalpy obtained in this work is -41.7 kJ/mol for the modified water model, which coincides with the experimental value [53], and -41.2 kJ/mol for the original TIP5P model, which is still closer to the experimental value than Paschek's result.

Table 3. Thermodynamic properties of pure water at 0.1 MPa. "TIP5P opt.": calculated with the modified TIP5P potential of this work; "TIP5P orig.": calculated with the original pair potential parameters [36]; "exp.": obtained from IAPWS reference equation of state [53].

T/K	method	V_m/cm^3 mol^{-1}	$\Delta_{vap}H_m$/kJ mol^{-1}	H_m^{res}/kJ mol^{-1}	μ_m^{res}/kJ mol^{-1}
298.15	TIP5P opt.	18.05 ± 0.1	44.2 ± 0.2	41.7 ± 0.1	23.06 ± 0.2
	TIP5P orig.	18.01 ± 0.1	43.7 ± 0.1	41.2 ± 0.1	22.72 ± 0.1
	exp.	18.07	43.99	41.73	26.47
303.00	TIP5P opt.	18.21 ± 0.1	43.7 ± 0.1	41.1 ± 0.1	22.67 ± 0.1
	TIP5P orig.	18.20 ± 0.2	43.5 ± 0.2	41.0 ± 0.1	21.91 ± 0.2
	exp.	18.09	43.78	41.57	26.22
308.00	TIP5P opt.	18.28 ± 0.1	42.7 ± 0.1	40.9 ± 0.2	22.04 ± 0.2
	TIP5P orig.	18.27 ± 0.1	43.6 ± 0.1	40.2 ± 0.2	21.34 ± 0.2
	exp.	18.12	43.56	41.38	25.97
313.00	TIP5P opt.	18.34 ± 0.1	43.5 ± 0.1	40.9 ± 0.1	21.59 ± 0.1
	TIP5P orig.	18.36 ± 0.2	42.5 ± 0.2	40.0 ± 0.1	20.86 ± 0.2
	exp.	18.16	43.35	41.19	25.72
318.00	TIP5P opt.	18.39 ± 0.1	43.4 ± 0.2	40.8 ± 0.1	21.14 ± 0.2
	TIP5P orig.	18.41 ± 0.1	42.1 ± 0.1	39.7 ± 0.1	20.32 ± 0.2
	exp.	18.19	43.14	40.86	25.48

Recently Rick presented a comparison of the original TIP5P and a modified TIP5P model which included different treatments of the long-range interactions [54] (reaction field and an Ewald sum method similar to the one used by Paschek); his results for the density of original TIP5P water agree with each other as well as with our results (see Table 3). The enthalpy and chemical potential values with the modified TIP5P water model are slightly closer to experimental results than the results computed with the original TIP5P water model at higher temperatures. It seems therefore likely that the deviations of Paschek's work were not caused by faulty long-range corrections, but by insufficient statistical averaging.

As explained before, the residual chemical potential of water was calculated by three different methods; the Widom insertion method, the Widom deletion method and the particle deletion scheme by Boulougouris *et al.* [49–52]. Fig. 1 depicts the results for the modified TIP5P water between 298.15 and 318 K at a pressure of 0.1 MPa. The Widom insertion method comes closest to the experimental results; it needs, however, 10–20 % more CPU time than the particle deletion schemes. That both particle deletion schemes give large deviations from the well-established insertion method is surprising. Both schemes had been tested before on the Lennard–Jones fluid and had been found to give satisfying results. But the deletion schemes fail for dense TIP5P water. This may be due to the fact that the removed water molecule is a soft molecule with long-range interactions, and evidently the bias introduced by particle deletion

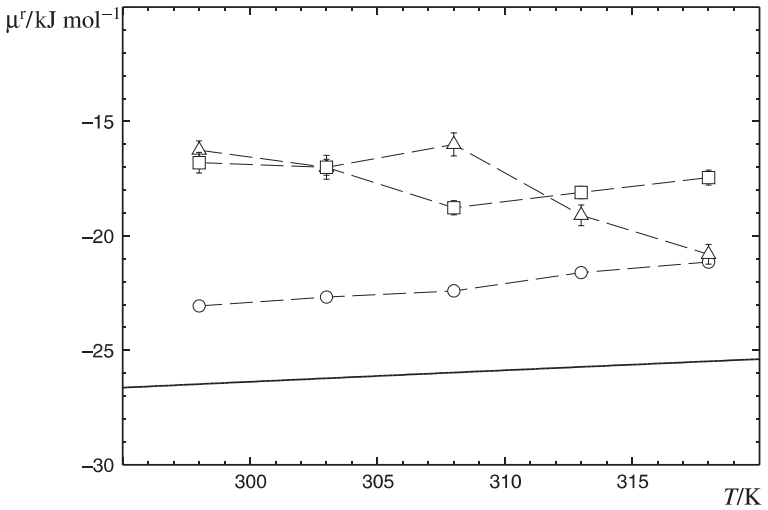

Fig. 1. The residual chemical potential of liquid water at 0.1 MPa with different methods: ○: Widom insertion method, △: Widom deletion method, □: Theodorou deletion method, — empirical equation of state (IAPWS).

could not be fully compensated. Similar systematic deviations of the deletion methods for molecules with long-range potentials have been also been observed by other authors [55, 56]; the phenomenon is recently under investigation.

Ji *et al.* determined the chemical potential of water at room temperature by molecular dynamics simulations and obtained a value of −23 kJ/mol [57]. Our Monte Carlo simulations with the Widom insertion method gave a value of −23.1 kJ/mol with the modified TIP5P water model (−22.7 kJ/mol with the original TIP5P water model), whereas the experimental value at room temperature is −26.5 kJ/mol [53].

Figs. 2–4 show the oxygen–oxygen, oxygen–hydrogen and hydrogen–hydrogen pair correlation functions of pure liquid water for temperatures between 298.15 and 318 K. A comparison of the location of the maxima and minima of the oxygen–oxygen pair distribution function with various water model simulations and experimental observations is given in Table 4. Table 5 lists simulation and experimental results for the peaks of the oxygen–hydrogen and hydrogen–hydrogen pair distribution functions.

It turns out that there are some discrepancies between previous simulation results from literature as well as between experimental results for the pair distribution functions of water. We observe, however, that the simulation results of this work agree well with the latest experimental data of Soper [58] and Head-Gordon and Hura [59]. Moreover, our results are also in good agreement with the *ab initio* calculations of Schwegler *et al.* [32].

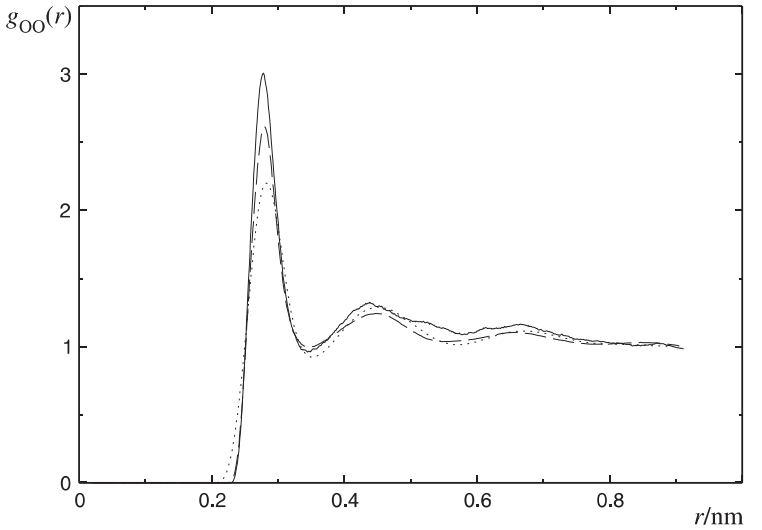

Fig. 2. The oxygen–oxygen pair distribution function of liquid water at 0.1 MPa. ——: 298.15 K, – – –: 308 K, · · · · ·: 318 K.

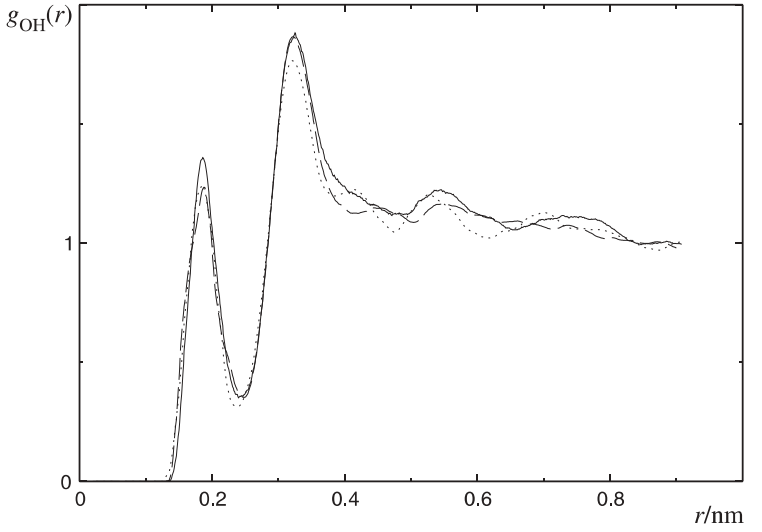

Fig. 3. The oxygen–hydrogen pair distribution function of water. For an explanation of the symbols see Fig. 2.

Differences in the height and the width of the first peak of the oxygen–oxygen pair distribution function indicate a change in the coordination number N_c. Head-Gordon and Hura [59] calculated values of 5.1, 5.2 and 4.7,

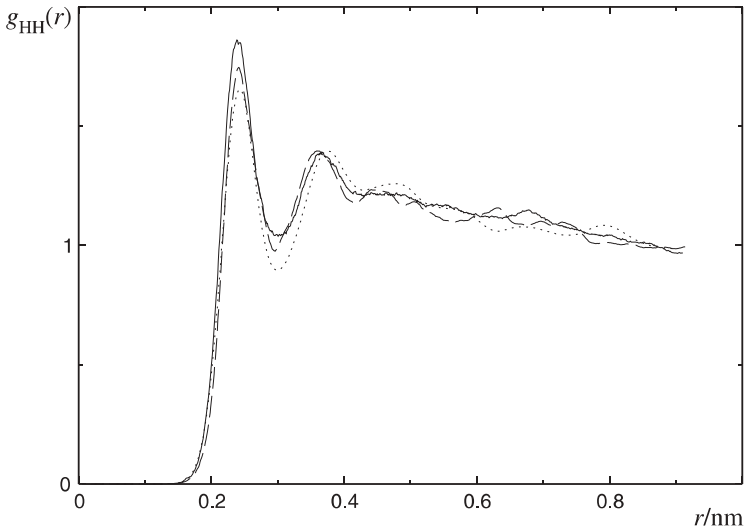

Fig. 4. The hydrogen–hydrogen pair distribution function of water. For an explanation of the symbols see Fig. 2.

Table 4. Extrema of the oxygen–oxygen pair distribution function of pure water, $g_{OO}(r)$, at 298.15 K and 0.1 MPa. Entries are in chronological order; "TIP5P opt." refers to this work.

source	1st peak		1st min.		2nd peak		2nd min.		3rd peak	
	r/Å	$g(r)$	r/Å	$g(r)$	r/Å	$g(r)$	r/Å	$g(r)$	r/Å	$g(r)$
simulation results										
ST2 [30]	2.8	3.2	3.5	0.7	4.6	1.2	5.7	0.9	6.9	1.1
SPC [68]	2.8	2.8	3.5	0.9	4.5	1.0	5.7	0.9	6.8	1.0
TIP5P orig. [36]	2.7	2.9	3.4	0.8	4.5	1.2	5.6	0.9	6.7	1.0
TIP5P opt.	2.9	2.9	3.4	0.8	4.5	1.2	5.5	1.0	6.6	1.1
experimental results										
Narten *et al.* [60]	3.0	2.2	3.5	0.8	4.5	1.2	5.6	0.9	6.9	1.1
ALS [59, 62, 69]	2.7	2.8	3.4	0.8	4.4	1.1	5.5	0.9	6.7	1.1
Soper *et al.* [58]	2.8	2.2	3.5	0.8	4.5	1.2	5.5	0.9	6.7	1.1

based on experiments by Narten *et al.* [60], Soper *et al.* [61], and Hura *et al.* [62], respectively. A coordination number below five indicates that liquid water preserves much of its ice-like tetrahedral structure, but with differences in hydrogen bonding patterns that would also include deformed hydrogen bonding [59]. Our value for the first hydration shell of the oxygen–oxygen pair

Table 5. Extrema of the oxygen–hydrogen and hydrogen–hydrogen pair distribution functions of pure water, $g_{OH}(r)$ and $g_{HH}(r)$ at 298.15 K and 0.1 MPa. "TIP5P opt." refers to this work, the data of Soper are experimental values.

source	$g_{OH}(r)$				$g_{HH}(r)$			
	1st peak		2nd peak		1st peak		2nd peak	
	r/Å	$g(r)$	r/Å	$g(r)$	r/Å	$g(r)$	r/Å	$g(r)$
TIP5P opt.	1.9	1.3	3.5	1.7	2.3	1.7	3.8	1.3
Soper 1996 [70]	1.9	1.6	3.3	1.5	2.5	1.2	3.9	1.1
Soper 2000 [58]	1.8	1.2	3.7	1.3	2.3	1.3	3.8	1.3

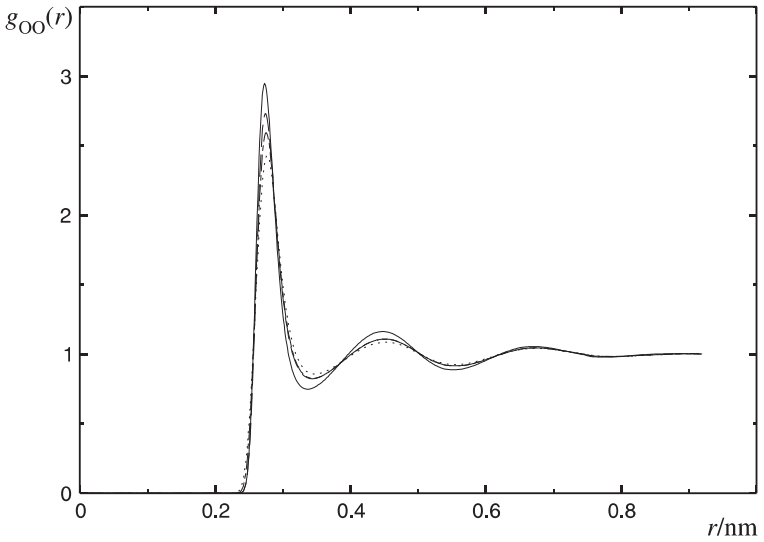

Fig. 5. The oxygen–oxygen pair distribution function of water containing methane (methane mole fraction 0.0917) at 0.1 MPa. —: 298.15 K, – – –: 308 K, – · –: 318 K, · · · · ·: 333 K. (These functions were computed with a significantly larger number of Monte Carlo moves than the corresponding distribution functions of pure water; hence the reduced statistical noise at long distances.)

distribution function is 4.8, which indicates a more structured liquid water, in agreement with the work of Head-Gordon and Hura.

3.2 Hydrophobic interactions

Figs. 5 and 8 show the oxygen–oxygen pair correlation functions of water in the water–methane and water–ethane systems. The first maximum of the oxygen–oxygen pair correlation function is higher for the water–ethane sys-

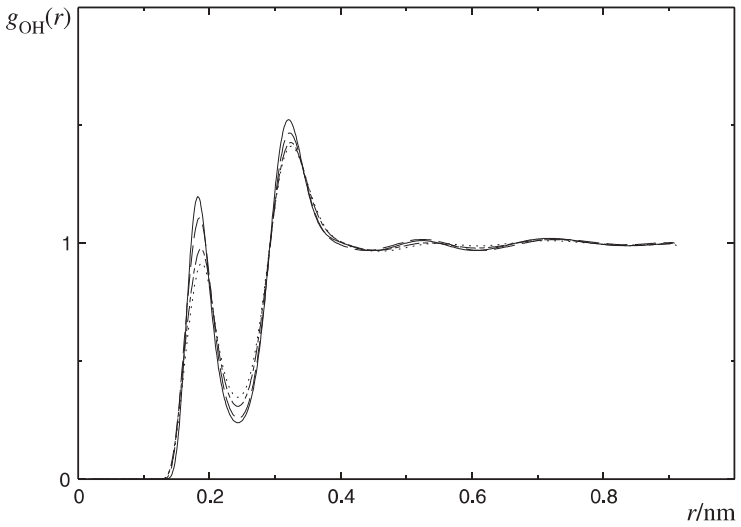

Fig. 6. The oxygen–hydrogen pair distribution function of water containing methane. For further explanations see Fig. 5.

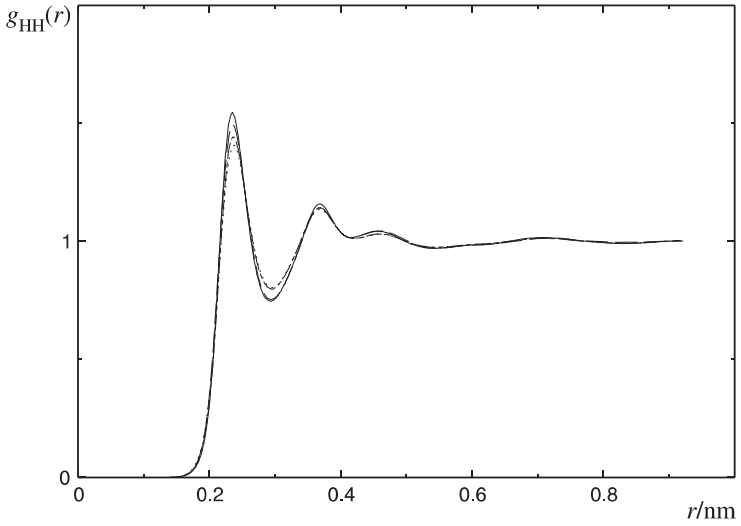

Fig. 7. The hydrogen–hydrogen pair distribution function of water containing methane. For further explanations see Fig. 5.

tem; the decrease of the peak height and outward shift of the peak with increasing temperature are more pronounced for this system, too. The second maximum of the oxygen–oxygen pair distribution function of water also shows

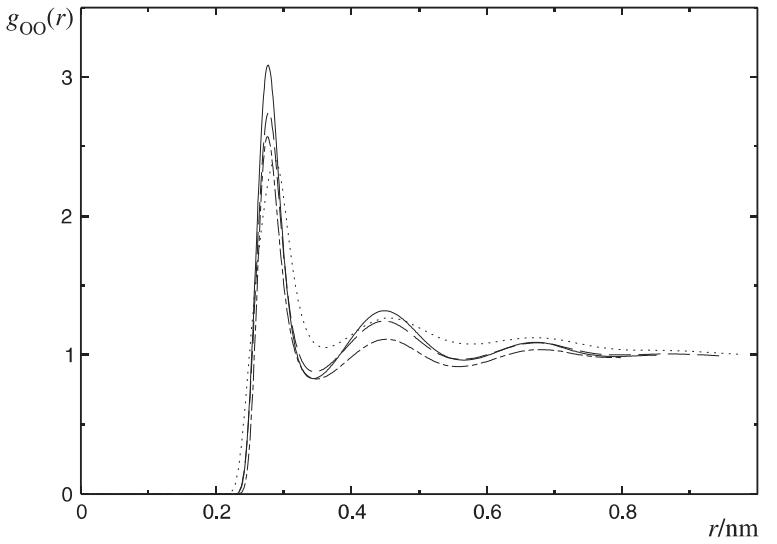

Fig. 8. The oxygen–oxygen pair distribution function of water containing ethane (ethane mole fraction 0.0917) at 0.1 MPa. —: 298.15 K, – – –: 308 K, – · –: 318 K, · · · · ·: 333 K.

a stronger temperature dependence for the water–ethane system than for the water–methane system (Figs. 5 and 8).

The behavior of the oxygen–hydrogen and hydrogen–hydrogen pair correlation functions is similar to that of the oxygen–oxygen function, as can be seen in Figs. 6–7 and 9–10. Table 6 shows the oxygen–hydrogen coordination numbers in the first hydration shell of bulk water as well as the water–methane and water–ethane systems. For the water–ethane system there is a slight increase in coordination number with comparison to bulk water at 298.15 K. For the water–methane system there is a slight decrease in the coordination number, which becomes more significant at higher temperatures, in agreement with the results of Dill *et al.* [63].

Table 7 presents the oxygen–hydrogen coordination numbers in the second hydration shell for bulk water and the water–methane and water–ethane systems. There is no increase of this coordination number in the water–ethane system with respect to bulk water as was observed for the first hydration shell. Instead, the coordination number decreases for bulk water as well as for the water–methane and water–ethane mixtures. The decrease becomes more significant with higher temperature for the water–ethane system. In general, these results are in agreement with the nuclear scattering findings of Koh *et al.*, which showed an overall decrease in hydrogen bonding between water molecules with increasing temperature in the vicinity of apolar molecules [64].

Table 8 shows the solute–solute coordination numbers for methane and ethane in water over a range of temperatures. The first shell coordination

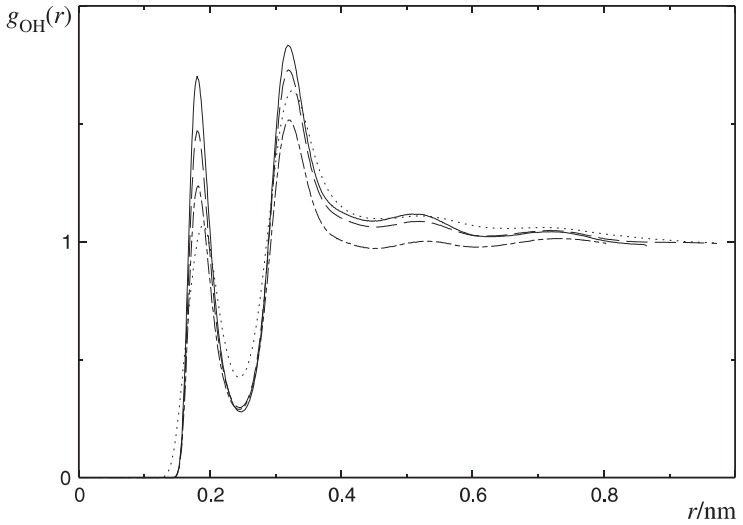

Fig. 9. The oxygen–hydrogen pair distribution function of water containing ethane. For further explanations see Fig. 8.

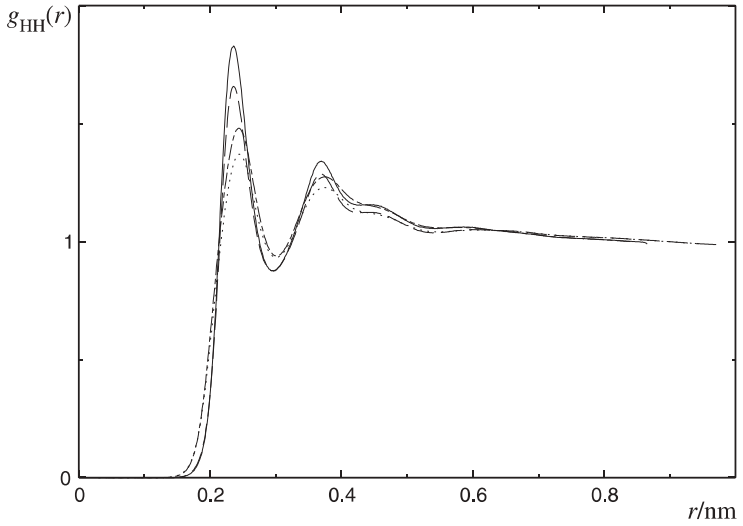

Fig. 10. The hydrogen–hydrogen pair distribution function of water containing ethane. For further explanations see Fig. 8.

number N_{c1}, calculated by integrating over the first peak of the pair distribution function, represents contact pairs, whereas the second shell coordination number, N_{c2}, represents solvent-separated pairs. Both systems show an in-

Table 6. Hydrogen bonding in the first hydration shell: O−H coordination number for various temperatures.

T/K	N_{c1}		
	bulk water	water + methane	water + ethane
298.15	3.3	3.2	3.5
303.00	3.3	3.2	3.4
308.00	3.2	3.0	3.3
313.00	3.2	2.9	3.2
318.00	3.2	2.8	3.2
323.00		2.8	3.2
328.00		2.8	3.1
333.00		2.7	3.1

Table 7. Hydrogen bonding in the second hydration shell: O−H coordination number for various temperatures.

T/K	N_{c2}		
	bulk water	water + methane	water + ethane
298.15	6.3	5.2	5.6
303.00	6.0	5.1	5.2
308.00	5.9	5.1	4.8
313.00	5.8	5.0	4.7
318.15	5.7	5.0	4.5
323.00		4.9	4.4
328.00		4.9	4.3
333.00		4.9	4.2

Table 8. Coordination numbers of methane and ethane in the first and second coordination shells.

	methane		ethane	
T/K	N_{c1}	N_{c2}	N_{c1}	N_{c2}
298.15	0.11	0.50	0.78	0.44
303.00	0.13	0.43	0.79	0.41
308.00	0.16	0.41	0.79	0.37
313.00	0.22	0.40	0.83	0.23
318.00	0.26	0.38	0.86	0.21
323.00	0.27	0.42	0.87	0.21
328.00	0.27	0.43	0.91	0.20
333.00	0.29	0.39	0.94	0.18

Table 9. Residual chemical potential of methane and ethane in water at 0.1 MPa predicted with the optimized TIP5P model.

T/K	$\mu^{\mathrm{res}}_{\mathrm{CH_4}}$/kJ mol^{-1}	$\mu^{\mathrm{res}}_{\mathrm{C_2H_6}}$/kJ mol^{-1}
298.15	9.12 ± 0.2	8.65 ± 0.1
303.00	9.16 ± 0.3	8.73 ± 0.1
308.00	9.41 ± 0.2	8.75 ± 0.1
313.00	9.66 ± 0.1	8.79 ± 0.3
318.00	9.99 ± 0.2	8.88 ± 0.2
323.00	10.04 ± 0.2	8.91 ± 0.1
328.00	10.09 ± 0.1	8.93 ± 0.1
333.00	10.11 ± 0.2	9.02 ± 0.2

creased tendency to form contact pairs with increasing temperature, which is more pronounced for ethane than for methane. These results are in partial agreement with the MB water model calculations of Dill *et al.*, who proposed that two small apolar molecules prefer a solvent-separated state, whereas larger solutes tend to get into contact at room temperature [63]. Furthermore, Smith and Haymet [20], Mancera and Buckingham [21] and Lüdemann *et al.* [23] also reported an increased tendency for small molecules to form contact pairs with increasing temperature, which is in agreement with our results.

The residual chemical potential of methane and ethane in water were calculated with the Widom insertion method; the results are shown in Table 9. The residual chemical potentials increase with temperature, which is in agreement with experiments. Furthermore, these results indicate that the solubility of these apolar molecules in water decreases with temperature since their chemical potential increases.

The simulated residual chemical potential of methane at 0.1 MPa with the modified TIP5P at 323 K is about 10 kJ/mol, whereas Paschek obtained a value of 9.4 kJ/mol at 325 K [41]; the experimental value is approximately 9.65 kJ/mol. Experimental data were obtained from Henry's constants according to Fernandez-Prini and Crovetto [65], employing the water densities from the IAPWS equation of state [53]. For ethane the simulation result is 8.6 kJ/mol at 298.15 K, whereas the experimental result is 7.6 kJ/mol [66].

The chemical potential calculations of nonpolar molecules in water show a strong dependence on the chosen model for the solutes as well as for water. Hernandez-Cobos *et al.* studied the hydration properties of methane using the OPLS model in TIP4P water and obtained a chemical potential of 31.4 kJ/mol at 300 K, which is larger than the experimental value [24]. This might be attributed to the difficulties associated with sampling the phase space. Gallicchio *et al.* calculated the chemical potential values for methane and ethane in TIP4P water, applying a perturbation method to the OPLS

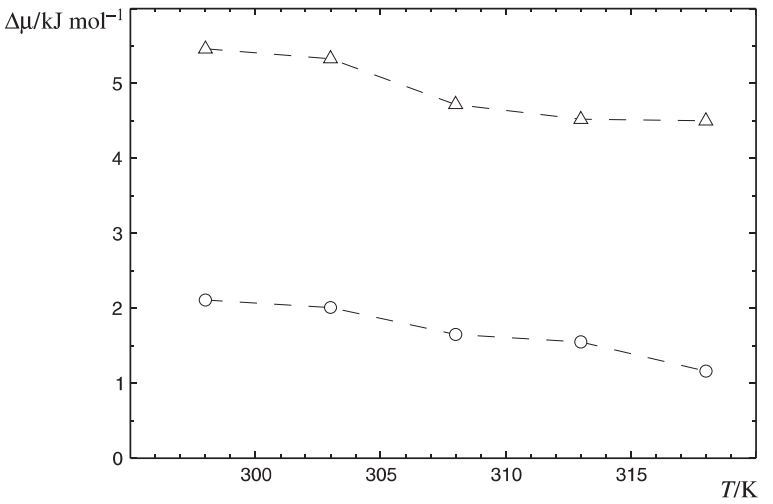

Fig. 11. Change of the chemical potential of liquid water at 0.1 MPa caused by the addition of a nonpolar solute. ○: methane, △: ethane.

models for the solutes, and obtained higher values than the experimental ones, too [67]. Ravishanker *et al.* used the MCY model for water and reported that the solvent-separated methane pair has a lower energy than the contact pair [19].

In order to study the effect of apolar solutes on water, it is interesting to consider the change of the chemical potential of water upon addition of the apolar species:

$$\Delta\mu = \mu_{\text{pure}} - \mu_{\text{mix}} \,. \tag{7}$$

Here μ_{mix} refers to the mixtures of 216 water and 2 apolar molecules studied in this work. The results are shown in Fig. 11. The change of the chemical potential of water $\Delta\mu$ is much larger with ethane than with methane. The residual chemical potential change of water together with the pair distribution functions indicate that the water molecules are more affected when the size of the apolar molecule increases.

4. Conclusion

The structural and thermodynamic properties of liquid water and of the dilute solutions of methane and ethane in water were studied by Monte Carlo simulations for different temperatures. A modified TIP5P model for water was developed which, although deviating only minimally from the original TIP5P

model, gives significantly better predictions of the liquid phase chemical potential and the enthalpy. The new model accurately describes the structural and thermodynamic properties of liquid water between 298.15 and 318 K at ambient pressure.

The hydrophobic interactions were investigated for various temperatures and for solutes of different size, namely methane and ethane. These nonpolar molecules show a tendency to aggregate that increases with temperature. Methane as a solute forms mostly solvent-separated pairs at low temperatures, but with increasing temperature contact pairs are preferred. However, for ethane the quota of contact pairs is always high. Our results are in agreement with previous results from molecular simulations [20–22, 63].

The oxygen–hydrogen coordination numbers of the water–methane and water–ethane systems, averaged over the whole ensemble, are less than those of bulk water. The decrease of the coordination number with temperature is more pronounced for the water–ethane system, which is probably due to the larger size of the ethane molecule. Furthermore, the change of the chemical potential for water in the vicinity of ethane molecules is more significant than with methane molecules. The calculated chemical potential values for methane and ethane increase with temperature, which indicates a lower solubility of these solutes with increasing temperature.

Simulations with the Widom insertion method, using the modified TIP5P model for water and OPLS models for apolar molecules yield chemical potential values in agreement with experimental data.

Acknowledgement

Financial support by the Fonds der chemische Industrie e.V. as well as INTAS (International Association for the Promotion of Cooperation with Scientists from the New Independent States of the Former Soviet Union, Project 640-00) is gratefully acknowledged.

References

1. M. Yaacobi and A. Ben-Naim, J. Phys. Chem. **78** (1974) 175.
2. E. E. Tucker and S. D. Christian, J. Phys. Chem. **83** (1979) 426.
3. R. P. Kennan and G. L. Pollack, J. Chem. Phys. **93** (1990) 2724.
4. J. A. V. Butler and W. S. Reid, J. Chem. Soc. **1936**(2) (1936) 1171.
5. J. A. V. Butler, Trans. Faraday Soc. **33** (1937) 229.
6. F. Franks, *Water: A Comprehensive Treatise*. Plenum Press, New York (1975).
7. H. S. Frank and M. W. Evans, J. Chem. Phys. **13** (1945) 507.
8. M. H. Abraham, J. Am. Chem. Soc. **104** (1982) 2085.
9. G. Némethy and H. A. Scheraga, J. Chem. Phys. **90** (1962) 3382.
10. M. S. Jhon, J. Grosh, T. Ree, and H. Eyring, J. Chem. Phys. **44** (1966) 1465.
11. D. C. Rapaport and H. A. Scheraga, J. Phys. Chem. **86** (1982) 873.

12. K. Watanabe and H. C. Andersen, J. Phys. Chem. **90** (1986) 795.
13. A. Laaksonen and P. Stilbs, Mol. Phys. **74** (1991) 747.
14. L. R. Pratt and D. Chandler, J. Chem. Phys. **67** (1977) 3683.
15. L. R. Pratt and D. Chandler, J. Chem. Phys. **73** (1980) 3434.
16. C. Pangali, M. Rao, and B. J. Berne, J. Chem. Phys. **71** (1979) 2975.
17. C. Pangali, M. Rao, and B. J. Berne, J. Chem. Phys. **71** (1979) 2982.
18. S. Swaminathan and D. L. Beveridge, J. Am. Chem. Soc. **101** (1979) 5832.
19. G. Ravishanker, M. Mezei, and D. L. Beveridge, Faraday Symp. Chem. Soc. **17** (1982) 79.
20. D. Smith and A. D. J. Haymet, J. Chem. Phys. **98** (1993) 6445.
21. R. L. Mancera and A. D. Buckingham, Chem. Phys. Lett. **234** (1995) 296.
22. L. X. Dang, J. Chem. Phys. **100** (1994) 9032.
23. S. Lüdemann, H. Schreiber, R. Abseher, and O. Steinhauser, J. Chem. Phys. **104** (1996) 286.
24. J. Hernández-Cobos, A. D. Mackie, and L. F. Vega, J. Chem. Phys. **114** (2001) 7527.
25. N. T. Skipper, Chem. Phys. Lett. **207** (1993) 424.
26. N. T. Skipper, C. H. Bridgeman, A. D. Buckingham, and R. L. Mancera, Faraday Discuss. **103** (1996) 141.
27. S. Shimizu and H. S. Chan, J. Chem. Phys. **113** (2000) 4683.
28. J. D. Bernal and R. H. Fowler, J. Chem. Phys. **1** (1933) 515.
29. H. Popkie, H. Kistenmacher, and E. Clementi, J. Chem. Phys. **59** (1973) 1325.
30. F. H. Stillinger and A. Rahman, J. Chem. Phys. **60** (1974) 1545.
31. K. S. Kim, B. J. Mhin, U.-S. Choi, and K. Lee, J. Chem. Phys. **97** (1992) 6649.
32. E. Schwegler, G. Galli, and F. Gygi, Phys. Rev. Lett. **84** (2000) 2429.
33. K. Coutinho, R. C. Guedes, B. J. Costa Cabral, and S. Canuto, Chem. Phys. Lett. **369** (2003) 345.
34. W. L. Jorgensen, J. Chandrasekhar, J. D. Madura, R. W. Impey, and M. L. Klein, J. Chem. Phys. **79** (1983) 926.
35. W. L. Jorgensen and J. D. Madura, Mol. Phys. **56** (1985) 1381.
36. M. W. Mahoney and W. L. Jorgensen, J. Chem. Phys. **112** (2000) 8909.
37. G. S. Kell, J. Chem. Eng. Data **20** (1975) 97.
38. C. A. Angell and H. Kanno, Science **193** (1976) 1121.
39. C. A. Angell, W. J. Sichina, and M. Oguni, J. Phys. Chem. **86** (1982) 998.
40. M. Lísal, J. Kolafa, and I. Nezbeda, J. Chem. Phys. **117** (2002) 8892.
41. D. Paschek, J. Chem. Phys. **120** (2004) 6674.
42. D. Frenkel and B. Smit, *Understanding Molecular Simulation*. Academic Press, London, 2nd edition (2002).
43. F. H. Stillinger, J. Phys. Chem. **74** (1970) 3677.
44. Gaussian98. Gaussian Inc., Wallingford, CT, USA (1998).
45. R. S. Fellers, C. Leforestier, L. B. Braly, M. G. Brown, and R. J. Saykally, Science **284** (1999) 945.
46. S. A. Clough, Y. Beers, G. P. Klein, and L. S. Rothman, J. Chem. Phys. **59** (1973) 2254.
47. W. L. Jorgensen, J. D. Madura, and C. J. Swenson, J. Am. Chem. Soc. **106** (1984) 6638.
48. M. P. Allen and D. Tildesley, *Computer Simulation of Liquids*. Clarendon Press, Oxford (1987).
49. B. Widom, J. Chem. Phys. **39** (1963) 2808.
50. N. G. Parsonage, Mol. Phys. **89** (1996) 1133.
51. N. G. Parsonage, J. Chem. Soc. Faraday Trans. **92** (1996) 1129.
52. G. C. Boulougouris, I. G. Economou, and D. N. Theodorou, J. Chem. Phys. **115** (2001) 8231.
53. W. Wagner and A. Pruß, J. Phys. Chem. Ref. Data **31** (2002) 387.

54. S. W. Rick, J. Chem. Phys. **120** (2004) 6085.
55. N. Lu and D. A. Kofke, in *Foundations of Molecular Modeling and Simulation*, P. Cummings and P. Westmoreland (Eds.), vol. 97 of AIChE Symp. Ser. AIChE (2001), p. 146.
56. D. Wu and D. A. Kofke, J. Chem. Phys. **123** (2005) 084109.
57. J. Ji, T. Cagir, and B. M. Pettitt, J. Chem. Phys. **96** (1992) 1333.
58. A. K. Soper, Chem. Phys. **258** (2000) 121.
59. T. Head-Gordon and G. Hura, Chem. Rev. **102** (2002) 2651.
60. A. H. Narten, W. E. Thiessen, and L. Blum, Science **217** (1982) 1033.
61. A. K. Soper, F. Bruni, and M. A. Ricci, J. Chem. Phys. **106** (1997) 247.
62. G. Hura, J. M. Sorenson, R. M. Glaeser, and T. Head-Gordon, J. Chem. Phys. **113** (2000) 9140.
63. K. A. Dill, T. M. Truskett, V. Vlachy, and B. Hribar-Lee, Annu. Rev. Biophys. Biomol. Struct. **34** (2005) 173.
64. C. A. Koh, R. P. Wisbey, X. P. Wu, R. E. Westmacott, and A. K. Soper, J. Chem. Phys. **113** (2000) 6390.
65. R. Fernandez-Prini and R. Crovetto, J. Phys. Chem. Ref. Data **18** (1989) 1231.
66. A. Ben-Naim and Y. Marcus, J. Chem. Phys. **81** (1984) 2016.
67. G. Gallicchio, M. M. Kubo, and R. M. Levy, J. Phys. Chem. B **104** (2000) 6271.
68. H. J. C. Berendsen, J. P. M. Postma, W. F. van Gunsteren, and J. Hermans, in *Intermolecular Forces: Proceedings of the 14th Jerusalem Symposium on Quantum Chemistry and Biochemistry*, B. Pullman (Ed.). Reidel, Dordrecht (1981), p. 331.
69. J. M. Sorenson, G. Hura, R. M. Glaeser, and T. Head-Gordon, J. Chem. Phys. **113** (2000) 9149.
70. A. K. Soper, Chem. Phys. **202** (1996) 295.